Performance of megahertz amplified optical time-stretch optical coherence tomography (AOT-OCT)

Jingjiang Xu, Xiaoming Wei, Luoqin Yu, Chi Zhang, Jianbing Xu, K. K. Y. Wong, and Kevin K. Tsia*

Department of Electrical and Electronic Engineering, The University of Hong Kong, Pokfulam Road, Hong Kong, China

*tsia@hku.hk

Abstract: Enabled by the ultrahigh-speed all-optical wavelength-swept mechanism and broadband optical amplification, amplified optical time-stretch optical coherence tomography (AOT-OCT) has recently been demonstrated as a practical alternative to achieve ultrafast A-scan rate of multi-MHz in OCT. With the aim of identifying the optimal scenarios for MHz operation in AOT-OCT, we here present a theoretical framework to evaluate its performance metric. In particular, the analysis discusses the unique features of AOT-OCT, such as its superior coherence length, and the relationship between the optical gain and the A-scan rate. More importantly, we evaluate the sensitivity of AOT-OCT in the MHz regime under the influence of the amplifier noise. Notably, the model shows that AOT-OCT is particularly promising when operated at the A-scan rate well beyond multi-MHz – not trivially achievable by any existing swept-source OCT platform. A sensitivity beyond 90 dB, close to the shot-noise limit, can be maintained in the range of 2 – 10 MHz with an optical net gain of ~10dB. Experimental measurement also shows excellent agreement with the theoretical prediction. While distributed fiber Raman amplification is mainly considered in this paper, the theoretical model is generally applicable to any type of amplification schemes. As a result, our analysis serves as a useful tool for further optimization of AOT-OCT system – as a practical alternative to enable MHz OCT operation.

OCIS codes: (110.4500) Optical coherence tomography; (110.4280) Noise in imaging systems; (120.3180) Interferometry.

References and links

1. D. Huang, E. A. Swanson, C. P. Lin, J. S. Schuman, W. G. Stinson, W. Chang, M. R. Hee, T. Flotte, K. Gregory, C. A. Puliafito, and J. G. Fujimoto, "Optical Coherence Tomography," Science **254**(5035), 1178–1181 (1991).
2. H. C. Lee, J. J. Liu, Y. Sheikine, A. D. Aguirre, J. L. Connolly, and J. G. Fujimoto, "Ultrahigh speed spectral-domain optical coherence microscopy," Biomed. Opt. Express **4**(8), 1236–1254 (2013).
3. L. An, P. Li, G. P. Lan, D. Malchow, and R. K. K. Wang, "High-resolution 1050 nm spectral domain retinal optical coherence tomography at 120 kHz A-scan rate with 6.1 mm imaging depth," Biomed. Opt. Express **4**(2), 245–259 (2013).
4. B. Potsaid, I. Gorczynska, V. J. Srinivasan, Y. L. Chen, J. Jiang, A. Cable, and J. G. Fujimoto, "Ultrahigh speed Spectral / Fourier domain OCT ophthalmic imaging at 70,000 to 312,500 axial scans per second," Opt. Express **16**(19), 15149–15169 (2008).
5. R. Wang, J. X. Yun, X. C. Yuan, R. Goodwin, R. R. Markwald, and B. Z. Gao, "Megahertz streak-mode Fourier domain optical coherence tomography," J. Biomed. Opt. **16**(6), 066016 (2011).
6. D. Choi, H. Hiro-Oka, H. Furukawa, R. Yoshimura, M. Nakanishi, K. Shimizu, and K. Ohbayashi, "Fourier domain optical coherence tomography using optical demultiplexers imaging at 60,000,000 lines/s," Opt. Lett. **33**(12), 1318–1320 (2008).
7. D. H. Choi, H. Hiro-Oka, K. Shimizu, and K. Ohbayashi, "Spectral domain optical coherence tomography of multi-MHz A-scan rates at 1310 nm range and real-time 4D-display up to 41 volumes/second," Biomed. Opt. Express **3**(12), 3067–3086 (2012).

#217247 - $15.00 USD Received 18 Jul 2014; revised 30 Aug 2014; accepted 1 Sep 2014; published 10 Sep 2014

8. W. Y. Oh, B. J. Vakoc, M. Shishkov, G. J. Tearney, and B. E. Bouma, "> 400 kHz repetition rate wavelength-swept laser and application to high-speed optical frequency domain imaging," Opt. Lett. **35**(17), 2919–2921 (2010).
9. R. Huber, M. Wojtkowski, and J. G. Fujimoto, "Fourier Domain Mode Locking (FDML): A new laser operating regime and applications for optical coherence tomography," Opt. Express **14**(8), 3225–3237 (2006).
10. B. Potsaid, B. Baumann, D. Huang, S. Barry, A. E. Cable, J. S. Schuman, J. S. Duker, and J. G. Fujimoto, "Ultrahigh speed 1050nm swept source / Fourier domain OCT retinal and anterior segment imaging at 100,000 to 400,000 axial scans per second," Opt. Express **18**(19), 20029–20048 (2010).
11. T. H. Tsai, B. Potsaid, Y. K. Tao, V. Jayaraman, J. Jiang, P. J. S. Heim, M. F. Kraus, C. Zhou, J. Hornegger, H. Mashimo, A. E. Cable, and J. G. Fujimoto, "Ultrahigh speed endoscopic optical coherence tomography using micromotor imaging catheter and VCSEL technology," Biomed. Opt. Express **4**(7), 1119–1132 (2013).
12. I. Grulkowski, J. J. Liu, B. Potsaid, V. Jayaraman, C. D. Lu, J. Jiang, A. E. Cable, J. S. Duker, and J. G. Fujimoto, "Retinal, anterior segment and full eye imaging using ultrahigh speed swept source OCT with vertical-cavity surface emitting lasers," Biomed. Opt. Express **3**(11), 2733–2751 (2012).
13. W. Wieser, B. R. Biedermann, T. Klein, C. M. Eigenwillig, and R. Huber, "Multi-Megahertz OCT: High quality 3D imaging at 20 million A-scans and 4.5 GVoxels per second," Opt. Express **18**(14), 14685–14704 (2010).
14. T. Klein, W. Wieser, L. Reznicek, A. Neubauer, A. Kampik, and R. Huber, "Multi-MHz retinal OCT," Biomed. Opt. Express **4**(10), 1890–1908 (2013).
15. S. Moon and D. Y. Kim, "Ultra-high-speed optical coherence tomography with a stretched pulse supercontinuum source," Opt. Express **14**(24), 11575–11584 (2006).
16. K. Goda, D. R. Solli, and B. Jalali, "Real-time optical reflectometry enabled by amplified dispersive Fourier transformation," Appl. Phys. Lett. **93**(3), 031106 (2008).
17. K. Goda, A. Fard, O. Malik, G. Fu, A. Quach, and B. Jalali, "High-throughput optical coherence tomography at 800 nm," Opt. Express **20**(18), 19612–19617 (2012).
18. T. J. Ahn, Y. Park, and J. Azana, "Ultrarapid Optical Frequency-Domain Reflectometry Based Upon Dispersion-Induced Time Stretching: Principle and Applications," IEEE J. Sel. Top. Quantum Electron. **18**(1), 148–165 (2012).
19. K. Goda, K. K. Tsia, and B. Jalali, "Serial time-encoded amplified imaging for real-time observation of fast dynamic phenomena," Nature **458**(7242), 1145–1149 (2009).
20. T. T. W. Wong, A. K. S. Lau, K. K. Y. Ho, M. Y. H. Tang, J. D. F. Robles, X. M. Wei, A. C. S. Chan, A. H. L. Tang, E. Y. Lam, K. K. Y. Wong, G. C. F. Chan, H. C. Shum, and K. K. Tsia, "Asymmetric-detection time-stretch optical microscopy (ATOM) for ultrafast high-contrast cellular imaging in flow," Sci. Rep. **4**, 3656 (2014).
21. H. W. Chen, C. Lei, F. J. Xing, Z. L. Weng, M. H. Chen, S. G. Yang, and S. Z. Xie, "Multiwavelength time-stretch imaging system," Opt. Lett. **39**(7), 2202–2205 (2014).
22. J. J. Xu, C. Zhang, J. B. Xu, K. K. Y. Wong, and K. K. Tsia, "Megahertz all-optical swept-source optical coherence tomography based on broadband amplified optical time-stretch," Opt. Lett. **39**(3), 622–625 (2014).
23. Y. Park, T. J. Ahn, J. C. Kieffer, and J. Azaña, "Optical frequency domain reflectometry based on real-time Fourier transformation," Opt. Express **15**(8), 4597–4616 (2007).
24. S. Tozburun, M. Siddiqui, and B. J. Vakoc, "A rapid, dispersion-based wavelength-stepped and wavelength-swept laser for optical coherence tomography," Opt. Express **22**(3), 3414–3424 (2014).
25. X. M. Wei, A. K. S. Lau, T. T. W. Wong, C. Zhang, K. K. M. Tsia, and K. K. Y. Wong, "Coherent Laser Source for High Frame-Rate Optical Time-Stretch Microscopy at 1.0 mu m," IEEE J. Sel. Top. Quantum Electron. **20**, 5 (2014).
26. M. E. Marhic, *Fiber Optical Parametric Amplifiers, Oscillators and Related Devices* (Cambridge University, 2007).
27. G. P. Agrawal, *Fiber-Optic Communication Systems,* 3rd ed. (Wiley, 2002).
28. K. Goda, D. R. Solli, K. K. Tsia, and B. Jalali, "Theory of amplified dispersive Fourier transformation," Phys. Rev. A **80**(4), 043821 (2009).
29. K. K. Tsia, K. Goda, D. Capewell, and B. Jalali, "Performance of serial time-encoded amplified microscope," Opt. Express **18**(10), 10016–10028 (2010).
30. B. R. Biedermann, W. Wieser, C. M. Eigenwillig, T. Klein, and R. Huber, "Dispersion, coherence and noise of Fourier domain mode locked lasers," Opt. Express **17**(12), 9947–9961 (2009).
31. Z. L. Hu, Y. S. Pan, and A. M. Rollins, "Analytical model of spectrometer-based two-beam spectral interferometry," Appl. Opt. **46**(35), 8499–8505 (2007).
32. M. A. Choma, M. V. Sarunic, C. H. Yang, and J. A. Izatt, "Sensitivity advantage of swept source and Fourier domain optical coherence tomography," Opt. Express **11**(18), 2183–2189 (2003).
33. D. R. Solli, J. Chou, and B. Jalali, "Amplified wavelength-time transformation for real-time spectroscopy," Nat. Photonics **2**(1), 48–51 (2008).
34. M. N. Islam, "Raman amplifiers for telecommunications," IEEE J. Sel. Top. Quantum Electron. **8**(3), 548–559 (2002).
35. K. Goda, A. Mahjoubfar, and B. Jalali, "Demonstration of Raman gain at 800 nm in single-mode fiber and its potential application to biological sensing and imaging," Appl. Phys. Lett. **95**(25), 251101 (2009).
36. A. Mahjoubfar, K. Goda, G. Betts, and B. Jalali, "Optically amplified detection for biomedical sensing and imaging," J. Opt. Soc. Am. A **30**(10), 2124–2132 (2013).
37. C. Headley and G. Agrawal, *Raman Amplification in Fiber Optical Communication Systems* (Academic Press, 2005).

#217247 - $15.00 USD Received 18 Jul 2014; revised 30 Aug 2014; accepted 1 Sep 2014; published 10 Sep 2014

38. H. Masuda, S. Kawai, and K. I. Suzuki, "Optical SNR enhanced amplification in long-distance recirculating-loop WDM transmission experiment using 1580 nm band hybrid amplifier," Electron. Lett. **35**(5), 411–412 (1999).
39. H. Masuda and S. Kawai, "Wide-band and gain-flattened hybrid fiber amplifier consisting of an EDFA and a multiwavelength pumped Raman amplifier," IEEE Photon. Technol. Lett. **11**(6), 647–649 (1999).
40. S. A. E. Lewis, S. V. Chernikov, and J. R. Taylor, "Characterization of double Rayleigh scatter noise in Raman amplifiers," IEEE Photon. Technol. Lett. **12**(5), 528–530 (2000).
41. American National Standards Institute, "American national standard for safe use of lasers," ANSI Z136.1–200 (ANSI, 2000).

1. Introduction

Optical coherence tomography (OCT) has proven to be a powerful noninvasive optical bioimaging modality because of its ability to offer label-free tissue tomographic and functional assessments in three-dimensional (3D) without relying on excisional biopsy and histopathology. It is found useful in clinical applications including ophthalmology, dermatology and gastroenterology to name a few [1]. These applications, in particular for those involving image-guided biopsy or surgery, very often demand for real-time 3D imaging, preferably at the video rate. To enable a complete volumetric OCT at such imaging speed, it is a mandate to realize an A-scan rate well beyond MHz – an unreachable speed regime with the current commercial-grade OCT systems, which typically run at ~1–10's kHz.

An assorted of technological advancements have been demonstrated for scaling the A-scan rate of OCT close to or even exceeding MHz. For instance, spectral domain OCT (SD-OCT) can now achieve the A-scan rate up to 100's kHz, beyond which is challenging because of the fundamental speed limitation of the line scan camera (CCD or CMOS cameras) [2–4]. It was reported that an effective A-scan rate of MHz can be realized by capturing the SD-OCT signal in a streak mode by a high-speed 2-dimensional CMOS camera and a synchronized streak resonant-scanning mirror [5]. It however requires relatively high illumination power and involves complicated scanning mirror synchronization to enable the streak mode. SD-OCT using an arrayed waveguide grating-type optical demultiplexer together with a photodiode arrays (with hundreds of single photodiodes) has also been demonstrated to achieve more than 10 MHz A-scan rate at the cost of considerably complex system configuration [6, 7]. On the other hand, swept-source OCT (SS-OCT) has been another attractive and practical OCT modality enabling fast A-scan rates. Over the past decade, the fundamental swept rate, i.e. A-scan rate, has to significantly boost to hundreds of kilohertz by the use of fast-rotating polygon scanning filter [8] or Fourier-domain mode locked (FDML) laser [9, 10]. SS-OCT based on vertical cavity surface emitting laser (VCSEL) [11, 12], or time-interleave of FDML pulses together with multi-spot illumination [13, 14] can further push the A-scan rate up to the MHz regime. Nevertheless, the high-speed wavelength-swept operations in these SS-OCT modalities all rely on mechanical moving parts (piezoelectric-driven Fabry-Pérot cavity, rotating-mirrors, or microelectromechanical system (MEMS)). The performance is thus inevitably subject to long-term mechanical stability.

An all-optical swept source based on *optical time-stretch* is a potential alternative as a robust inertia-free wavelength-swept mechanism enabling ultrahigh speed and long term SS-OCT operation [15–18]. In optical time-stretch (also known as dispersive Fourier transform) [19–22], a broadband pulse is optically wavelength-swept (or time-stretched) by group velocity dispersion (GVD) in a dispersive fiber (e.g. dispersion compensated fiber (DCF), or chirped fiber Bragg grating), with no mechanical wavelength-swept mechanism. The A-scan rate is thus governed by the repetition rate of the laser pulse train, which is typically 10's MHz for most of the broadband pulse lasers. However, optical time-stretch had not been widely accepted as an effective approach for SS-OCT until now. It is primarily because that previous work on time-stretch-based OCT had insufficient bandwidth (~10 nm) to provide practical axial resolution of OCT [16, 17, 23], and poor sensitivity (< 40 dB) [15]. Recently, we have demonstrated a practical time-stretch OCT modality, called amplified optical time-stretch OCT (AOT-OCT) which achieves tissue bioimaging with a record high sensitivity above 80 dB at an A-scan rate as high as 7.14 MHz [22]. The key attribute enabling such

#217247 - $15.00 USD Received 18 Jul 2014; revised 30 Aug 2014; accepted 1 Sep 2014; published 10 Sep 2014

performance is the implementation of *broadband* optical amplification in-line with the time-stretch process. It compensates the intrinsic optical loss, and even provides net optical gain, in the dispersive fiber and thus considerably enhances the sensitivity of OCT. We also note that a recent work demonstrated the potential of a high-speed wavelength-stepped laser for MHz AOT [24]. It showed that such novel laser design based on intracavity pulse stretching and compression using specialty GVD engineering can achieve a swept rate of 9 MHz.

Further improvement of the AOT-OCT performance requires in-depth understanding of the roles of key determining parameters in the system. The effects of the optical amplification and the associated noise are in particular critically governing the sensitivity of AOT-OCT. Yet, they have not been investigated in detailed in the prior work. Therefore, in this paper, we present a general theoretical framework evaluating the performance of AOT-OCT, with an aim of identifying the optimal scenarios for MHz operation in AOT-OCT. Specifically, we will discuss the unique features of AOT-OCT, such as its superior coherence length, and the relationship between the optical gain and the A-scan rate. More importantly, we will evaluate the sensitivity of AOT-OCT in the MHz regime under the influence of the optical amplification noise. While the theoretical model presented in this paper can be generically applicable to any types of optical amplifiers, we will particularly consider the use of distributed fiber Raman amplification (FRA) because of its unique advantages over other amplification schemes for optical time-stretch operation. Our model reveals that the amplifier noise critically affects the sensitivity of the AOT-OCT and has to be carefully controlled in order to optimize the imaging quality. The experimental measurement shows excellent agreement with the theoretical prediction. The model also shows that AOT-OCT is uniquely favorable for multi-MHz operation in term of attaining practical OCT sensitivity for bioimaging applications (> 90dB). We anticipate that the present study could provide a comprehensive insight for designing a robust AOT-OCT system as a practical SS-OCT alternative running in the MHz regime.

2. Theoretical model of AOT-OCT

Figure 1 shows the general schematic of an AOT-OCT system based on a Mach-Zehnder interferometer (MZI) with two couplers, a circulator and a fiber delay line. The *all-optical* swept-source employed in this system is derived from a broadband pulsed laser which can be generated either by supercontinuum generation in a highly-nonlinear fiber [22] or by the dispersion-managed fiber mode-locking [25]. The broadband spectrum of the pulse (with a bandwidth of few tens to hundreds of nanometers) is then mapped into the wavelength-swept temporal waveform in a dispersive fiber via GVD. This is the process called optical time-stretch. To counteract the dispersive loss in the fiber, the wavelength-swept waveform is optically amplified in order to enhance the OCT sensitivity. In its generic form, the optical amplification scheme could be implemented before, during and/or after the time-stretch process. There is no strict requirement on the type of amplifiers adopted in the system. It includes rare-earth-doped fiber amplifier (e.g. erbium-doped fiber amplifier (EDFA) for 1.5 μm operation, or ytterbium-doped fiber amplifier (YDFA) for 1 μm operation), semiconductor optical amplifier (SOA), fiber Raman amplifier (FRA), or fiber optical parametric amplifier (FOPA) [26]. It can also be a multi-stage amplifier system based on either the same amplifier type or the hybrid amplifier type. It is known in the realm of telecommunication that the design criteria of the amplification scheme in such swept-source closely relates to its overall noise performance [27] which ultimately influences the OCT sensitivity (as discussed in the later section). As a consequence of the AOT, a rapidly wavelength-swept waveform with a repetition rate well above the megahertz regime (governed by the typical pulsed laser source) is generated as the light source for AOT-OCT. In the AOT-OCT system, we utilize a fiber-based MZI which consists of a fiber coupler splitting the swept-source light into the reference arm and sample arm. The AOT-OCT interferograms are acquired by recombining the reference and sample arm signals by another coupler, and are then captured by a photodetector. While balanced detection could further be

#217247 - $15.00 USD Received 18 Jul 2014; revised 30 Aug 2014; accepted 1 Sep 2014; published 10 Sep 2014

improved the OCT sensitivity, we here employ a single photodetector for the sake of simplicity in our AOT-OCT theoretical model.

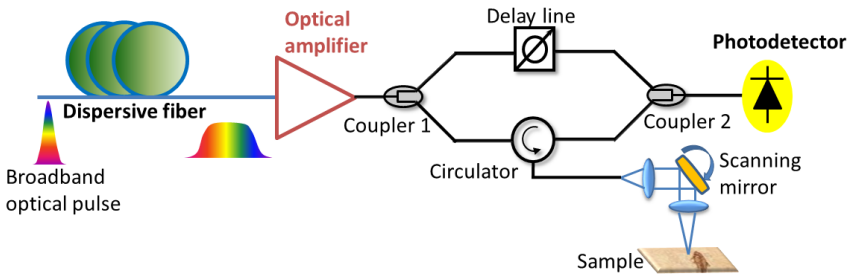

Fig. 1. Schematic of a generic AOT-OCT system.

2.1 Instantaneous linewidth of AOT-OCT

Similar to all the SS-OCT modalities, the instantaneous linewidth of the AOT swept-source determines the intrinsic roll-off performance of AOT-OCT. Given that the GVD is large enough (i.e. in the far-field regime of optical time-stretch [28]), such instantaneous linewidth or equivalently the spectral resolution originates from the ambiguity in the wavelength-to-time mapping process. It means that not only one wavelength contributes to the temporal waveform at any one time point. Such spectral resolution can be estimated by stationary phase approximation (SPA) which is defined as [29]:

$$\delta\lambda_{SPA} = \lambda\sqrt{\frac{2}{D\cdot c}}, \tag{1}$$

where λ is the center wavelength of the light source, $D = D_c L$ is the total dispersion of the dispersive fiber (typically in ns/nm) with a length of L (in km) and a GVD coefficient of D_c (in ps/km-nm), c is the speed of light in vacuum. Note that Eq. (1) does not take into account the higher-order GVD coefficients which are essential for recalibrating the nonlinear wavelength-to-time mapping. Nevertheless, Eq. (1) provides sufficiently good approximation to estimate the achievable spectral resolution and thus the roll-off performance.

In AOT-OCT, the A-scan rate is essentially equivalent to the repetition rate of the laser. It imposes the upper bound of the required total dispersion D_{max}, beyond which the consecutive wavelength-swept (time-stretched) waveforms overlap each other. Here we define D_{max} when the 3 dB bandwidth of the time-stretched waveform occupies 80% of the interval of the adjacent waveforms. It means that D_{max} has an inverse relationship with the A-scan rate, which is expressed as. $D_{\max} = \dfrac{0.8}{f_A \Delta\lambda}$, where f_A is the A-scan rate, $\Delta\lambda$ is the bandwidth of the light source. Thus, the coherence length l_c of AOT-OCT, which is another parameter quantifying the roll-off performance, is given by (assuming a Gaussian spectral shape):

$$l_c = \frac{2\ln 2}{\pi}\frac{\lambda^2}{\delta\lambda_{SPA}}. \tag{2}$$

Figure 2 shows the general trends of the spectral resolution and coherence length for different A-scan rates, particularly in the megahertz regime. From Eqs. (1)-(2), it is clear that there is a trade-off between the A-scan rate and the spectral resolution. It means that scaling the A-scan rate compromises the coherence length in AOT-OCT. Nevertheless, a coherence length as long as centimeter can be achieved at an A-scan rate close to 10MHz. Such coherence length is significantly longer than that achieved in typical SS-OCT which depends on the spectral resolution of the tunable filter [13, 30]; and SD-OCT which depends on the

#217247 - $15.00 USD Received 18 Jul 2014; revised 30 Aug 2014; accepted 1 Sep 2014; published 10 Sep 2014

pixel resolution of the image sensor [31]. Therefore, the long coherence length achieved in AOT-OCT makes it attractive for long depth-range imaging in the megahertz regime. In general, apart from the wavelength-to-time mapping ambiguity (characterized by SPA-limited resolution, i.e. Eq. (1)), the spectral resolution of the AOT-OCT can also be governed by another limiting factor, which is the temporal resolution (or equivalently the electrical bandwidth) of the photodetector [28, 29]. In this limiting regime, the spectral resolution is given by $\delta\lambda_{\mathrm{det}} = 0.35/(D_{\max}\cdot B_{\mathrm{e}})$. Consider the megahertz A-scan rates (from 1 – 10 MHz), the required detection bandwidth Be should be beyond 1 GHz (assuming there are 2000 sample points), according to Nyquist sampling criterion. The corresponding spectral resolution imposed by the detection bandwidth is well below 40 pm and is smaller than the SPA-limited resolution for the A-scan rate exceeding 1MHz. Therefore, the actual spectral resolution of a multi-MHz AOT-OCT system should be primarily governed by the SPA-limited resolution as long as the detection bandwidth is sufficiently wide (>1GHz).

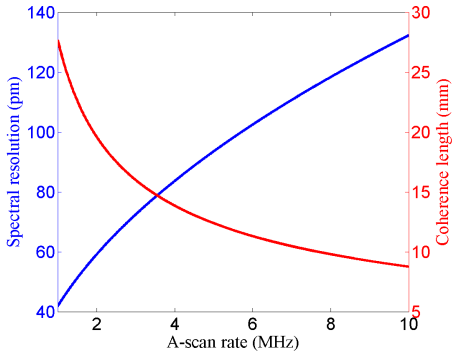

Fig. 2. Coherence length and spectral resolution as a function of A-scan rate in AOT-OCT. The center wavelength is 1620 nm and the optical bandwidth is 80 nm. The D_{max} is determined by $0.8/(f_A\Delta\lambda)$ in the unit of ns/nm.

2.2 Signal-to-noise (SNR) and sensitivity of AOT-OCT

The key feature of AOT-OCT is the use of broadband optical amplification to overcome the optical loss in the dispersive fiber and thus to enhance the sensitivity in the system. Assuming that the AOT process can provide a net optical power gain of G to the input signal which has the average power of P_{in}, the total power input to the OCT system is thus GP_{in}. Using a coupler and a circulator to guide the light into the sample arm, the power incident on the sample is $C_1T_cGP_{in}$, where C_1 is the power coupling ratio to the sample arm and T_c is the one-way transmission through circulator to the sample. Consider a mirror with a reflectivity of R_s is placed in the sample arm and the transmission of fiber delay line in reference arm is T_d, the optical powers captured at the photodetector from the reference arm and the sample arm are $P_r = (1-C_1)(1-C_2)T_dGP_{in} = T_rGP_{in}$ and $P_s = C_1C_2T_c^2R_sGP_{in} = T_sGP_{in}$, respectively, where $T_r = (1-C_1)(1-C_2)T_d$ and $T_s = C_1C_2T_c^2R_s$ are the power transmission in the reference arm and the sample arm. C_2 is the power coupling ratio of the coupler 2 before the photodetector.

As a result, we can write the photocurrent detected in the AOT-OCT system as:

$$i_d = \rho[T_rGP_{in} + T_sGP_{in} + 2GP_{in}\sqrt{T_rT_s}\cos(2k\Delta z)], \qquad (3)$$

where ρ is the detector responsivity (in A/W), k is the optical wavenumber which will be mapped into time-space via GVD, thus has a relationship of $k = k_0 - 2\pi(t-t_0)/D\lambda_0^2$ by

#217247 - $15.00 USD Received 18 Jul 2014; revised 30 Aug 2014; accepted 1 Sep 2014; published 10 Sep 2014

neglecting higher-order GVD coefficients (k_0, λ_0, t_0 are the center wavenumber, center wavelength and the corresponding time position of the stretched pulse), Δz is the optical path length difference between the two arms. The expression of the AOT-OCT signal is given by the interference term, i.e. the third term of Eq. (3):

$$i_s = 2\rho G P_{in} \sqrt{T_r T_s} \cos(2k\Delta z). \tag{4}$$

Following the conventional definition, the SNR of AOT-OCT is obtained by considering the Fourier transform of the interference signal term and the noise variance. In this way, the mean-square peak signal at the position of Δz after the Fourier transform can be written as [32]:

$$\left\langle \tilde{i}_s \right\rangle^2 = \rho^2 T_r T_s (G P_{in})^2 M^2, \tag{5}$$

where M is the number of sample points assuming higher-order dispersion is negligible, i.e. the wavelength-swept waveform is evenly stretched. To evaluate the Fourier transform of the noise variance, we assume that all noise sources have a white noise characteristic. The uncorrelated noise variances are added incoherently in the discrete Fourier transform summation, giving rise $\widetilde{\sigma^2_{noise}} = M\sigma^2_{noise}$, where σ^2_{noise} is given by

$$\sigma^2_{noise} = T_t^2 \sigma^2_{am} + \sigma^2_{sh} + \sigma^2_{re}, \tag{6}$$

where $T_t = T_r + T_s$ is the total transmission in the interferometer. The total noise variances includes: (1) Shot noise $\sigma^2_{sh} = 2eI_{dc}B_e$ which follows the Poisson process. $I_{dc} = \rho(T_r + T_s)GP_{in}$ is the mean photodetector photocurrent. e is elementary electric charge. B_e is the electrical detection bandwidth; (2) Receiver noise $\sigma^2_{re} = NEP^2 \cdot B_e$, where the NEP is noise-equivalent power (NEP) (in $A/\sqrt{Hz}$); (3) Amplifier noise σ^2_{am} is evaluated depending upon different types of amplification mechanisms, which will be further discussed in the next section. As a result, the signal-to-noise ratio (SNR) of an AOT-OCT system can be generically given by:

$$SNR_{AOTOCT} = \left\langle \tilde{i}_s \right\rangle^2 / \widetilde{\sigma^2_{noise}} = \frac{\rho^2 T_r T_s (G P_{in})^2 M}{T_t^2 \sigma^2_{am} + 2e\rho T_t G P_{in} B_e + \sigma^2_{re}}. \tag{7}$$

The sensitivity of AOT-OCT is defined as reciprocal of the minimal sample reflectivity $R_{s,\min}$, at which the SNR equals one, i.e. $S_{AOTOCT} = 1/R_{s,\min}$. Similar to most of the OCT systems, it is typical for $R_s \ll 1$ that we can neglect the reflected power from the sample arm for sensitivity estimation. Thus, the total transmission can be simply expressed as $T_t = T_r + T_s \approx T_r$. Based on this approximation, the sensitivity of AOT-OCT system can be expressed as:

$$S_{AOTOCT} = \frac{\rho^2 T_r T_{s,0} (G P_{in})^2 M}{T_r^2 \sigma^2_{am} + 2e\rho T_r G P_{in} B_e + \sigma^2_{re}}, \tag{8}$$

where $T_{s,0} = C_1 C_2 T_c^2$ is the transmission of sample arm with a sample reflection of $R_s = 1$. Note that the detection bandwidth B_e should be bounded by the Nyquist–Shannon sampling criterion, i.e. $B_e = f_s/2$. Here, f_s is the data sampling rate which can be related to the A-scan rate f_A by $f_s = Mf_A$.

#217247 - $15.00 USD Received 18 Jul 2014; revised 30 Aug 2014; accepted 1 Sep 2014; published 10 Sep 2014

2.3 Noise analysis of AOT-OCT based on fiber Raman amplification

Optical amplification plays a decisive role in an AOT-OCT system particularly in terms of enhancing its sensitivity in the megahertz A-scan regime. As it is mentioned earlier that a number of fiber amplification schemes can generally be adopted in AOT-OCT, e.g. EDFA, YDFA, SOA, FOPA and FRA. Among them, FRA, particularly *distributed* FRA, possesses several key advantages over other amplification schemes for optical time-stretch operation. They include: (i) the widely tunable Raman gain spectrum depending upon the available pump wavelengths; (ii) its naturally broadband gain spectrum allowed by the amorphous nature in optical glass fiber; (iii) the gain bandwidth can be further broadened by using multi-wavelength pump lasers. Note also that broadband gain spectra can be realized using incoherent pump sources [33]; (iv) the noise figure of FRA is superior to rare-earth doped fiber amplifiers and SOAs [34–36]. By choosing the proper pump sources and dispersive fibers, all these FRA features are favorable for high-quality AOT-OCT in a wide wavelength range, spanning from 1μm to 1.5μm – the common window of OCT-based bioimaging applications. In this section, we will further investigate how the noise in FRA influences the SNR and thus the sensitivity performance of AOT-OCT, based on Eq. (8).

To evaluate the sensitivity of AOT-OCT based on FRA, it is necessary to model the Raman gain and the relevant noise sources in FRA. Similar analysis for biomedical sensing and imaging based on FRA has been discussed in [36]. For the sake of completeness, we here lay down the key considerations for AOT-OCT. Assuming no pump depletion and the signal-induced cross-phase modulation (XPM), the Raman gain (optical intensity gain) along the dispersive fiber is given by [37]:

$$G(z) = \exp\left[g_R \int_0^z I_p(z)dz - \alpha_s z \right], \tag{9}$$

where g_R is the Raman gain coefficient in the dispersive fiber, $I_p(z)$ is the pump intensity at the position z in the dispersive fiber. α_s is the linear propagation loss of the fiber (in km^{-1}). Consider a dispersive fiber with a length of L and the case of bidirectional pumping, we can obatin $I_p(z) = I_f(0)\exp(-\alpha_p z) + I_b(\mathrm{L})\exp[-\alpha_p(L-z)]$, where $I_f(0)$ and $I_b(\mathrm{L})$ are the input pump intensities of the forward and backward pumps at the two fiber ends, i.e. at $z = 0$ and $z = L$. These two input intensities can be expressed as:

$$I_f(0) = \frac{P_f(0)}{\pi(d_p/2)^2}, I_b(L) = \frac{P_b(L)}{\pi(d_p/2)^2}, \tag{10}$$

where $P_f(0)$ and $P_b(L)$ are the input pump powers in the forward and backward directions, respectively, and d_p is the mode field diameter of the pump in the dispersive fiber.

There are several factors that may influence the noise performance for FRA. We will describe all the noise sources in terms of variance of photocurrent generated by detector. The main noise sources (noise variances) of a distributed FRA include [37]:

(a) The variance of double Rayleigh backscattering (DRB) noise. This noise arises from a time-delayed crosstalk with the amplified signal light which is scattered backward and then forward in the fiber. This DRB noise can be expressed as:

$$\sigma_{DRB}^2 = 2 f_{DRB}[\rho G(L) P_{in}]^2, \tag{11}$$

where $f_{DRB} = r_s^2 \int_0^L G^{-2}(z) \int_z^L G^2(z')\mathrm{dz'dz}$ is the faction of the crosstalk-to-signal by DRB in the fiber. r_s is the Rayleigh backscattering coefficient.

(b) The variance of pump-to-Stokes relative intensity noise (RIN) transfer which can be estimated as:

#217247 - $15.00 USD Received 18 Jul 2014; revised 30 Aug 2014; accepted 1 Sep 2014; published 10 Sep 2014

$$\sigma_{RIN}^2 = [\rho G(L) P_{in}] \int_0^{B_e} RIN_s(f) df, \tag{12}$$

where the complete transfer function of the pump RIN to the Stokes $RIN_s(f)$ can be found in [36].

(c) The variance of amplified spontaneous emission (ASE) noise. The spectral density of the ASE in Raman amplifier is defined by $S_{ASE} = n_{sp} h \upsilon_s g_R G(L) \int_0^L \left[I_p(z) / G(z) \right] dz$, where the inversion parameter $n_{sp} = \left\{ 1 - \exp\left[-h(\upsilon_p - \upsilon_s) / (k_B T_f) \right] \right\}^{-1}$ [37]. Here k_B is the Boltzmann constant, h is Planck constant, T_f is the temperature in the fiber. υ_s and υ_p are the optical frequencies of the signal (Stokes) and pump, respectively. There are two different beating noise sources related to ASE: One is the beating noise of signal with ASE:

$$\sigma_{s-ASE}^2 = 4\rho^2 G(L) P_{in} S_{ASE} B_e. \tag{13}$$

The other one is the beating noise of ASE with itself:

$$\sigma_{ASE-ASE}^2 = 4\rho^2 S_{ASE}^2 B_e (B_o - \frac{B_e}{2}), \tag{14}$$

where B_o is the optical bandwidth of the photodetector.

The total noise of FRA is the summation of the aforementioned noise sources:

$$\sigma_{am}^2 = \sigma_{DRB}^2 + \sigma_{RIN}^2 + \sigma_{s-ASE}^2 + \sigma_{ASE-ASE}^2. \tag{15}$$

Substituting Eq. (15) into Eqs. (7) or (8), we can evaluate the SNR or sensitivity of AOT-OCT based on FRA. Again, the amplifier noise term in Eqs. (7) and (8) is a generic term describing the noise mechanisms of any type or form of optical amplification scheme, including the hybrid configuration (i.e. a multistage amplification combining different type of optical amplifiers [22, 38, 39]). Hence, by identifying the relevant noise sources of the employed optical amplification scheme, one can evaluate the corresponding SNR and sensitivity of the AOT-OCT based on Eqs. (7) and (8).

3. Results and discussion

3.1 The effect of coupling ratio on the sensitivity of AOT-OCT

It is evident that the terms T_r and $T_{s,0}$ in Eq. (8) depend on coupling ratios of the couplers in the MZI. To exemplify the influence of the coupling ratios on the AOT-OCT sensitivity and SNR, we here assume that the two couplers have the same coupling ratios, i.e. $C_1 = C_2$ and evaluate the sensitivity such AOT-OCT system running at an A-scan rate of 5 MHz based on Eq. (8). Other practical values of the parameters adopted in this analysis are detailed in the caption of Fig. 3, which shows the sensitivity as a function of the coupling ratio. We mainly investigate three main amplification conditions: (i) Net gain of G = 10 dB without amplifier noise (i.e. $\sigma_{am}^2 = 0$ for an ideal amplifier); (ii) Net gain of G = 10 dB with the amplifier noise from −30dB to −20dB of the input power (e.g. for −30dB amplifier noise, it means $\sigma_{am}^2 = (10^{-3} \rho G P_{in})^2$); (iii) No amplification, i.e. net gain G is replaced by dispersive loss of −10 dB in the fiber.

In general, adjusting the coupling ratio between 0 and 1 results in order-of-magnitude variation in sensitivity. In particular, a maximum sensitivity as high as ~90dB can be achieved when the coupling ration is ~0.9 in both cases (i) and (ii). More importantly, the essential role of amplification is clearly illustrated in Fig. 3. Employing amplification in AOT-OCT can easily improve the AOT-OCT sensitivity by at least 20 dB. It is primarily

#217247 - $15.00 USD Received 18 Jul 2014; revised 30 Aug 2014; accepted 1 Sep 2014; published 10 Sep 2014

because of that optical amplification overcomes the inherent dispersive loss during the optical time-stretch process within the long dispersive fiber.

3.2 The effect of the FRA performance on the sensitivity of AOT-OCT

In this section, we will investigate how the noise performance of FRA affects the sensitivity and thus the SNR of the AOT-OCT, particularly in the ultrafast A-scan regime, i.e. the A-scan rate beyond MHz. The parameter values adopted in the analysis are listed in Table 1. In particular, we chose the coupling ratios $C_1 = C_2 = 0.9$ as they give high sensitivity based on the analysis described in Section 3.1.

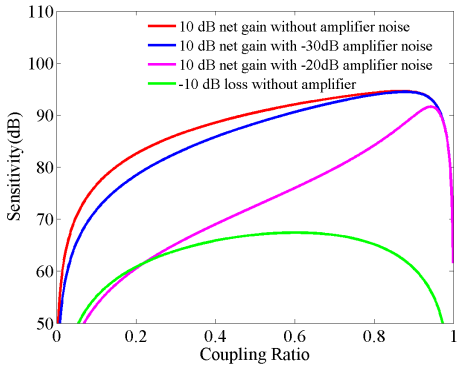

Fig. 3. AOT-OCT Sensitivity (A-scan rate of 5MHz) as a function of the MZI coupling ratio. The input power is 0.5mW. The electrical bandwidth of the detector is 5 GHz with a responsivity of $\rho = 1A/W$ and a noise-equivalent power of $NEP = 2pA/\sqrt{Hz}$. The delay line transmission $T_d = 0.8$, the circulator transmission $T_c = 0.85$,and the number of sampling points $M = 2000$.

Table 1. Parameter Values for Sensitivity Evaluation of AOT-OCT Based on FRA

Parameter	Value	Parameter	Value
Detector responsivity	$\rho = 1A/W$	Group velocity at Stokes wavelength	$v_s = 2.037777\times10^8 m/s$
Elementary charge	$e = 1.60218\times10^{-19} C$	Group velocity at pump wavelength	$v_p = 2.033867\times10^8 m/s$
Noise-equivalent power	$NEP = 2pA/\sqrt{Hz}$	GVD	$D_c = -100(ps/nm)/km$
Delay line transmission	$T_d = 0.8$	Mode field diameter at Stokes wavelength	$d_s = 6.01\mu m$
Circulator transmission	$T_c = 0.85$	Mode field diameter at pump wavelength	$d_p = 5.84\mu m$
Number of sampling points	$M = 2000$	Forward pump RIN	$RIN_p^f = 10^{-13} Hz^{-1}$
Planck constant	$h = 6.62607\times10^{-34} J\cdot s$	Backward pump RIN	$RIN_p^b = 10^{-13} Hz^{-1}$
Boltzmann constant	$k_B = 1.38065\times10^{-23} J/K$	Temperature of Raman gain medium (fiber)	$T_f = 293K$
Fiber attenuation at pump wavelength	$\alpha_p = 1.482\times10^{-4} m^{-1}$	Rayleigh backscattering coefficient	$r_s = 8.3804\times10^{-5} km^{-1}$
Fiber attenuation at Stokes wavelength	$\alpha_s = 1.485\times10^{-4} m^{-1}$	Optical bandwidth	$B_o = 9.145THz$
Stokes wavelength	$\lambda_s = 1620nm$	Coupling ratio	$C_1 = C_2 = 0.9$
Pump wavelength	$\lambda_p = 1520nm$		

#217247 - $15.00 USD Received 18 Jul 2014; revised 30 Aug 2014; accepted 1 Sep 2014; published 10 Sep 2014

Figure 4 shows how the AOT-OCT sensitivity generally scales with the input signal power. In the FPA scheme, we incorporate both the forward and backward pumps with the equal powers ($P_f(0) = P_b(L) = 240$ mW) such that the net optical gain of $G = 10$ dB is achieved in a 20-km long dispersive fiber (with $D_c = -100$ ps/nm/km, see Table 1). For small input signal (below 0 dBm), FRA can provide the sensitivity enhancement as high as ~45 dB, compared to the time-stretch operation without FRA – clearly demonstrating the pivotal role of optical amplification in AOT-OCT. The sensitivity of AOT-OCT is however saturated (at ~95 dB) at high input powers. It is mainly because that the optical gain is counteracted by the progressively stronger DRB and RIN in FRA when the input signal power is high [36]. Note that at the input power of ~0 dBm, the system approaches to shot-noise limited operation with a sensitivity as high as ~95dB. Here the shot-noise limited operation (i.e. the red curve in Fig. 4) is defined as $S_{AOTOCT,shot} = \rho T_{s,0} G P_{in} / e f_A$.

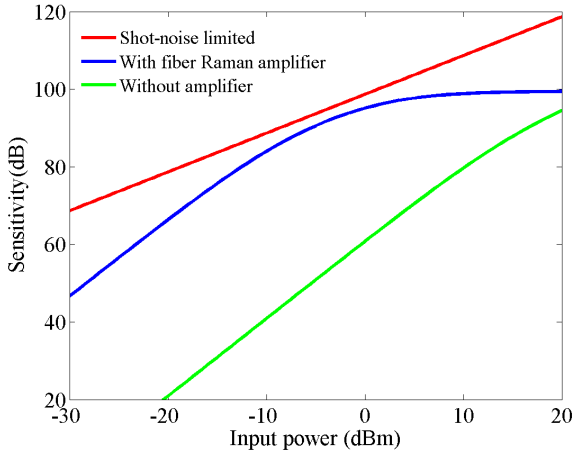

Fig. 4. AOT-OCT sensitivity as a function of input signal power. We consider the AOT-OCT system operating at 5 MHz A-scan rate using a photodetector with a bandwidth of 5 GHz. In this optical amplification scheme based on FRA, we incorporate both the forward and backward pumps with the equal powers of 240 mW such that the net optical gain of $G = 10$ dB is achieved in a 20-km long dispersive fiber (with $D_c = -100$ ps/nm/km, see Table 1).

We next investigate how the sensitivity is affected by FRA gain as well as the A-scan rate. It is now straightforward to expect, on one hand, higher optical gain leads to improved sensitivity. On the other hand, faster A-scan rate generally scales down the sensitivity because of loss of collected light signal in a shorter A-scan time window. Notwithstanding these two general trends, there is subtle relationship between the required A-scan rate and the given FRA gain in AOT-OCT – a unique feature absent in all other typical swept-source OCT modalities and could influence the sensitivity performance, which is shown in Fig. 5.

In the earlier section, we define the duty cycle of the swept-source to be 80% (with a time-stretch bandwidth of 80 nm) for practical AOT-OCT operation regardless the A-scan rate. It implies that for a given GVD of the dispersive fiber, the fiber length has to be adjusted to ensure the 80% duty-cycle of the time-stretched pulses (or wavelength-swept waveforms) at a certain A-scan rate. Varying the fiber length however also requires the change in FRA pump power if the net gain is meant to be fixed across different A-scan rates. The contour plot in Fig. 5(a) shows the required total FRA pump powers as a function of the net FRA gain as well as the A-scan rate in the MHz regime. As expected, generally less pump power is required for the shorter fiber length, and thus higher A-scan rate for a given net gain.

As described in Section 2.3, variation in pump power of FRA directly translates to that in the amplifier noise (see Eqs. (11)-(14)), and thus the overall sensitivity of AOT-OCT. Based on the sensitivity analysis described in Section 2 (i.e. Eq. (8)), a contour plot of AOT-OCT sensitivity as a function of net gain and A-scan rate can be obtained (Fig. 5(b)), similar to Fig.

#217247 - $15.00 USD Received 18 Jul 2014; revised 30 Aug 2014; accepted 1 Sep 2014; published 10 Sep 2014

5(a). From the plot, a sensitivity of more than 90 dB with the net gain of 10 – 15dB can be achieved at the A-scan rates of 2-10 MHz. Notably, it is preferable and practical to operate AOT-OCT beyond 2 MHz as it requires less pump powers (less than 30 dBm total pump power) to achieve the same 10 – 15dB gain (see Fig. 5(a)). It makes AOT-OCT uniquely suitable for practical MHz OCT – not trivially achievable by any existing SS-OCT platforms.

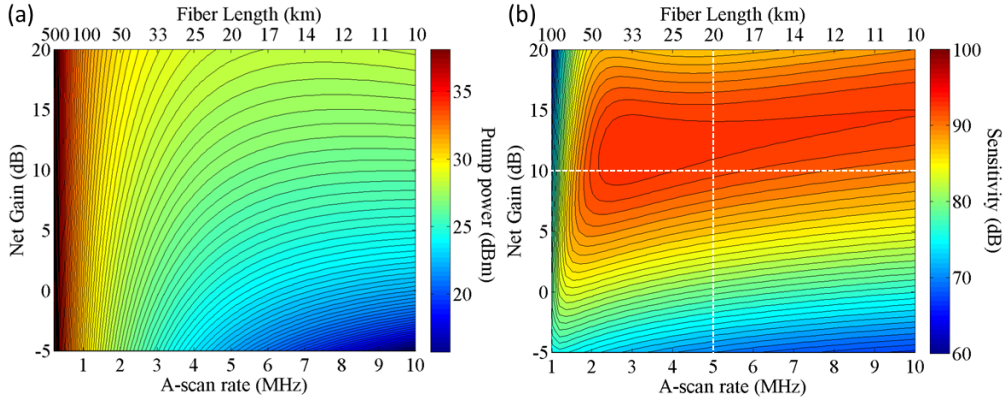

Fig. 5. (a) Required total pump powers for FRA and (b) the corresponding AOT-OCT sensitivity as a function of net optical gain and the A-scan rate. The input signal power is P_{in} = 0.5 mW. Other key parameters adopted in this analysis are specified in Table 1. In (b), the horizontal dashed line indicates the AOT-OCT sensitivity as a function of A-scan rate at a fixed net (FRA) gain of 10 dB (further elaborated in Fig. 6). On the other hand, the vertical dashed line indicates the AOT-OCT sensitivity as a function of net (FRA) gain at a fixed A-scan rate of 5 MHz (further elaborated in Fig. 7).

The advantage of operating AOT-OCT well above the MHz regime can be further appreciated in Fig. 6 which shows the case of constant net gain of 10 dB (i.e. the horizontal dashed line indicated in Fig. 5(b)). For the A-scan rate of less than 1 MHz, the required dispersive fiber length for the AOT process has to be hundreds of kilometer, which demands for very high pump powers >> 30 dBm, and thus introduces significant amplifier noise (particularly due to DRB noise [37]). Hence, the sensitivity drops significantly below 1 MHz. Operating at 2 – 10 MHz, AOT-OCT can achieve close-to-shot-noise-limited regime and maintains the sensitivity as high as > 90 dB – practical for most clinical and research-grade *in vivo* imaging [14]. Without the FRA implementation (green curve in Fig. 6), the power of output light is too weak because of the dispersive fiber loss. It thus results in a poor sensitivity, more than 30 dB worse than AOT-OCT. We note that the AOT-OCT sensitivity can be further improved and approach closer to the shot-noise limit by constructing isolated multistage FRA to suppress the DRB [40]. Such multistage and multiple-pump (more than 2) FRA configuration is not assumed in our model for simplicity.

#217247 - $15.00 USD Received 18 Jul 2014; revised 30 Aug 2014; accepted 1 Sep 2014; published 10 Sep 2014

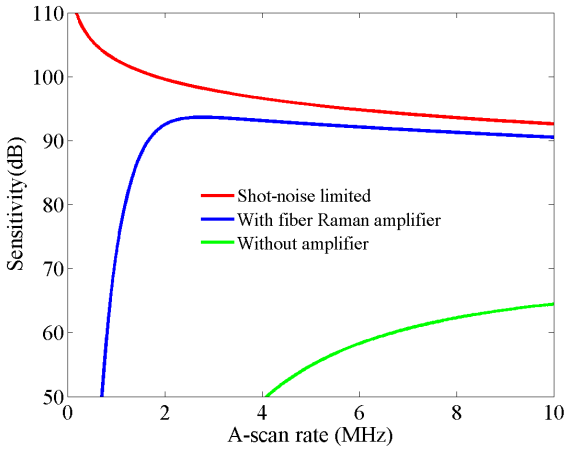

Fig. 6. AOT-OCT sensitivity (blue) as a function the A-scan rate at a fixed net (FRA) gain of 10 dB. It is also compared to the case of shot-noise limited AOT-OCT operation (red) as well as the case of AOT-OCT without optical amplification (green). Other key parameters adopted in this analysis are specified in Table 1.

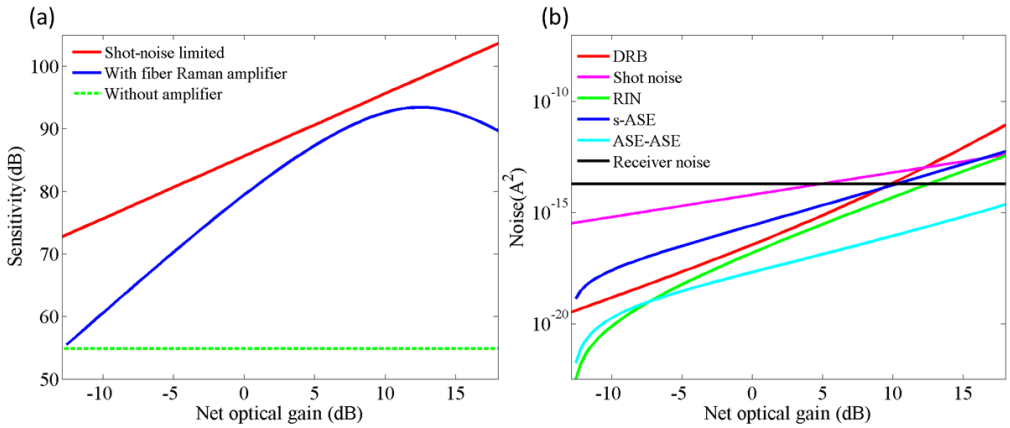

Fig. 7. (a) Sensitivity and (b) the corresponding noise components at the photodetector as a function the net FRA gain at a fixed A-scan rate of 5 MHz. Other key parameters adopted in this analysis are specified in Table 1.

To study the sensitivity dependence on the net FRA gain, we focus on the case of 5 MHz A-scan rate as shown in Fig. 7 (i.e. the vertical dashed line in Fig. 5(b)). In the range of small FRA gain, the receiver noise is the dominant factor (see Fig. 7(b)) determining the sensitivity of AOT-OCT which is considerably below the shot-noise limited sensitivity. As the FRA gain increases, the sensitivity is enhanced and approaches to the shot-noise limit (red curve in Fig. 7(a)). Once again, implementation of amplification in AOT-OCT is crucial as it enhances the signal level and thus the sensitivity. However, the DRB noise takes over to be the limiting factors of the sensitivity as the FRA gain continues to increase beyond 10 dB (see Fig. 7(b)). Other factors such as gain saturation and pump depletion will also become non-negligible in the high FRA gain regime. These effects explain why the sensitivity drops when the FRA scales beyond 10-15 dB (see the blue curve in Fig. 7(a)). Nevertheless, the critical role of amplification in AOT-OCT is well exemplified in Fig. 7(a) that the sensitivity can only be < 60 dB without the use of FRA. This clearly explains why the prior work on time-stretch-based OCT without amplification scheme was unable to perform in vivo biological imaging (e.g [15].). We also note that the illumination power on the sample should be limited within the safety standard, such as ANSI [41]. Assuming continuous illumination, the incident power

#217247 - $15.00 USD Received 18 Jul 2014; revised 30 Aug 2014; accepted 1 Sep 2014; published 10 Sep 2014

level onto the skin in the multi-MHz AOT-OCT should be kept below 10 mW [41]. Therefore, the net optical gain for an input power of 0.5 mW in our AOT-OCT system should not exceed 14 dB. Within this safety limit, the optical gain enables the sensitivity as high as 90 dB sensitivity at the A-scan rate of 5 MHz (see Fig. 7(a)).

3.3 Experimental sensitivity measurement of AOT-OCT

We here experimentally measure the sensitivity of an AOT-OCT system to verify the present theoretical model, as shown in Fig. 8. The light source is a femtosecond mode-lock fiber laser centered at 1560 nm with a bandwidth of ~50 nm and a repetition rate of 11 MHz. In this case, we have 1.5 mW input signal power for time-stretch in a DCF with the length of 10.6 km. And the Rayleigh backscattering coefficient of the DCF for the bandwidth near 1560 nm is about 10^{-4} km^{-1}. We use the 50/50 couplers to split and recombine the beams in the MZI configuration (Fig. 1). The electrical bandwidth of our photodetector is 15 GHz with 30 $pA/\sqrt{Hz}$ NEP. We put a mirror in the sample arm and measure the SNR by calculating the ratio between the peak of the point spread function (PSF) amplitude and the noise floor in dB scale (i.e 20 times the logarithmic scale of this ratio). Here, we implement the fiber optical amplification by launching a single pump laser for FRA into the DCF in the forward direction. As the FRA gain increases, the optical power from the reference and sample arms for detection may exceed the upper limit of the photodetector's dynamic range. To prevent power saturation or photodetector damage, we keep the power reflected from the sample arm as low as 0.25 μW by tilting the angle of the sample mirror and introduce an additional loss of −16 dB in the reference arm. Except the parameters described in this section, all other experimental parameters can be found in the Table 1. Based on the single-pump configuration, the model gives the very agreement with calculated sensitivity based on the experimental measurements as shown in Fig. 8(a). In particular, the theoretical model predicts well the degradation in sensitivity when the gain exceeds ~16 dB. It is mainly due to that the DBR noise becomes increasingly dominant and impairs the improvement of sensitivity in the present AOT-OCT system. The sensitivity improvement is also experimentally verified by the AOT-OCT images shown in Fig. 8(b) and 8(c) – when the gain is increased up to 15dB. However, the AOT-OCT image becomes noisier when the gain scales up to 19 dB (Fig. 8(d)), consistent with the drop in sensitivity shown in Fig. 8(a).

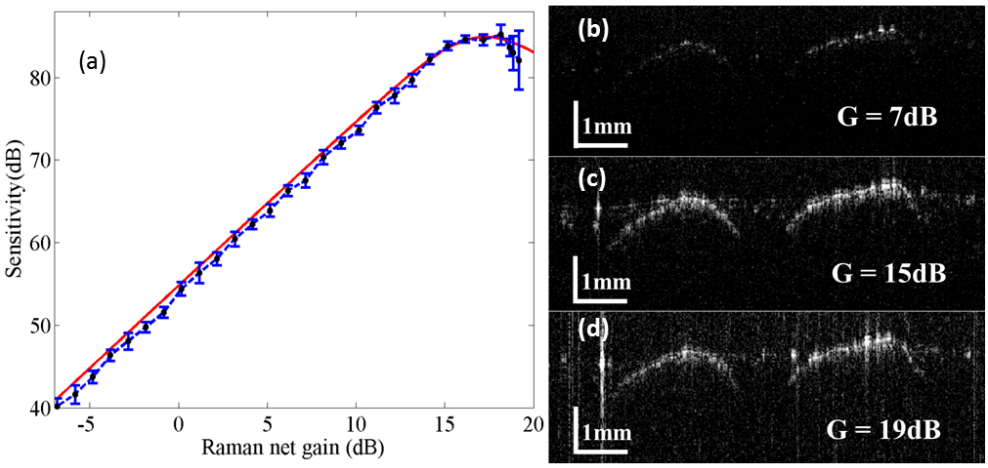

Fig. 8. (a) Measured and theoretical sensitivity in AOT-OCT system based on FRA. The solid red line is obtained by the theoretical model whereas the solid black circles are the calculated sensitivity based on experimental measurement in AOT-OCT system. The error bars represent a standard-deviation of the measured sensitivity in 20 repeated measurements. (b-d) AOT-OCT cross-sectional images of kiwifruit taken with a net FRA gain of 7dB, 15dB and 19 dB, respectively.

#217247 - $15.00 USD Received 18 Jul 2014; revised 30 Aug 2014; accepted 1 Sep 2014; published 10 Sep 2014

4. Concluding remarks

We have presented a theoretical model to evaluate the performance of an AOT-OCT system, particularly in the multi-MHz A-scan rate regime. As an all-optical SS-OCT modality, AOT-OCT can achieve a coherence length as long as ~10 mm even the A-scan rate is increased up to ~10 MHz. Using the MZI configuration, the sensitivity can be optimized by choosing the proper splitting ratios of the couplers. More importantly, the sensitivity is critically determined by the optical amplifier gain as well as the associated amplifier noise sources. Clearly the theoretical model reveals the essential role of amplification for enhancing the sensitivity. In addition, we have discussed a unique feature absent in all other typical SS-OCT modalities and could influence the sensitivity performance, i.e. the subtle relationship between required A-scan rate and the given FRA gain in AOT-OCT. Proper FRA gain and the length of the dispersive fiber has to be carefully taken into account for sensitivity optimization, as revealed in Fig. 5. Notably, the model also shows that AOT-OCT is particularly promising when operated at the A-scan rate well beyond multi-MHz – not trivially achievable by any existing SS-OCT platforms. A sensitivity beyond 90 dB, close to the shot-noise limit, can be maintained in the range of 2 – 10 MHz with an optical net gain of ~10dB. The theoretical model has also been validated by the experimental measurements, which showed excellent agreement in sensitivity with the model. Although only FRA is considered as the amplification scheme in the paper, the theoretical model can also be applicable to any type of optical amplifiers, such as EDFA, YDFA, SOA, FOPA. It can also be extended to the hybrid amplifier configuration (i.e. a multistage amplification combining different type of optical amplifiers [22, 38, 39]). As a result, the analysis discussed here is expected to serve as a useful tool for further optimization of AOT-OCT system – as a practical alternative to enable MHz OCT operation.

Acknowledgments

This work was partially supported by grant from the Research Grants Council of the Hong Kong SAR, China (Project No. HKU 7172/12E, 717510E, 717911E, 720112E) and University Development Fund of HKU.

#217247 - $15.00 USD Received 18 Jul 2014; revised 30 Aug 2014; accepted 1 Sep 2014; published 10 Sep 2014